Synthesis and Characterization of Sr-doped $LaFeO_3$ perovskite by sol-gel auto-combustion method

IOP Conf. Series: Journal of Physics: Conf. Series **1259** (2019) 012017 doi:10.1088/1742-6596/1259/1/012017

Synthesis and Characterization of Sr-doped $LaFeO_3$ perovskite by sol-gel auto-combustion method

M Kaewpanha[1,*], T Suriwong[1,*], W Wamae[2] and P Nunocha[1]

[1] School of Renewable Energy and Smart Grid Technology, Naresuan University, Phitsanulok 65000, Thailand
[2] Renewable Energy Technology Department, Faculty of Science Technology and Agriculture, Yala Rajabhat University, Yala 95000, Thailand

*Corresponding author: malineek@nu.ac.th, tawats@nu.ac.th

Abstract. In the present study, $La_{1-x}Sr_xFeO_3$ (x = 0.0, 0.2, 0.4, 0.6 and 0.8) perovskite was successfully prepared by sol-gel auto-combustion method. The prepared samples were characterized by X-ray diffraction (XRD), Field-emission scanning electron microscope (FESEM) with energy dispersive spectrum (EDS), Fourier transform infrared spectroscopy (FTIR) and spectrofluorometer. XRD and FESEM show that the prepared Sr-doped $LaFeO_3$ is single phase perovskite and nanosize with relatively homogeneous particle size distribution. Moreover, FESEM-EDS mapping analysis also exhibits the uniform distribution of all elements. The effect of Sr content in $LaFeO_3$ on the structure and morphology was also investigated. As results, the increasing of Sr content only affects the Fe-O stretching mode of $LaFeO_3$ perovskite, while it has little effect on the particle size and morphology of the Sr-doped $LaFeO_3$.

1. Introduction

Perovskite-type oxides of general formula ABO_3 (A = rare or alkali earth metals, B = transition metals) have become one of the most promising candidates due to their wide range of physical and technological properties, such as ferroelectricity, piezoelectricity, pyroelectricity, high-temperature superconductivity, magnetic behavior, and catalytic activity [1]. These properties determine the use of such materials in many applications such as gas transducers, catalysts, solid electrolyte batteries and magnetic sensors [2]. Among perovskite-type oxides, $LaFeO_3$ (LFO) is of interest because of its low price, non-toxicity, abundant reserve, and excellent electrochemical capacity [3]. Moreover, doping $LaFeO_3$ with divalent metal at A-site and transition metals at B-site affects its structural, transport, and electrical properties [3-5].

There are several methods for the synthesis of perovskite-type oxide $LaFeO_3$ such as solid-state reaction, sol-gel method, co-precipitation, and hydrothermal process [6-10]. Although solid-state reaction is the most common preparation method for $LaFeO_3$ powder, the synthesis occurs at high temperature (>1000 °C), resulting in powder products of non-porous, irregular shape, uncontrolled particle size and low surface area [7, 11]. Alternative methods to solid-state reaction methods such as sol-gel method, co-precipitation, and hydrothermal process, etc. have been reported to synthesize materials with better control of particle size and morphology [6, 8-10]. In addition, sol-gel auto-combustion is widely used for the preparation of inorganic ceramic and composite materials, with controlled properties for several applications [12, 13]. This is a novel way with a combination of the chemical sol–gel process and the combustion process. The advantages of sol–gel auto-combustion

include: inexpensive precursors; a simple preparation method; and a resulting nano-sized, homogeneous, highly reactive powder [14]. Therefore, the sol-gel auto combustion method has been considered as an attractive and quality technique for the preparation of oxide materials. However, no such reports have been found in literature on the synthesis of undoped and Sr-doped $LaFeO_3$ (LSF) materials by the sol-gel auto-combustion method.

In this work, therefore, we focus on the synthesis of undoped and Sr-doped $LaFeO_3$ (LSF) by sol-gel auto-combustion method. The synthesized LSF powder also were characterized by XRD, FESEM-EDS, FTIR and spectrofluorometer.

2. Experimental

2.1 Materials

Analytical grade lanthanum nitrate hexahydrate ($La(NO_3)_3 \cdot 6H_2O$, Lobachemie, India), iron nitrate nonahydrate ($Fe(NO_3)_3 \cdot 9H_2O$, Lobachemie, India), strontium nitrate ($Sr(NO_3)_2$, Himedia, India), citric acid ($C_6H_8O_7$, Lobachemie, India), and ethylene glycol ($C_2H_6O_2$, Lobachemie, India) were used as reagents for synthesis.

2.2 Synthesis of LSF powders

In this work, $La_{1-x}Sr_xFeO_3$ with x = 0.0, 0.2, 0.4, 0.6, 0.8, were prepared by the sol-gel auto-combustion method. Firstly, lanthanum nitrate hexahydrate, strontium nitrate and iron nitrate nonahydrate were weighted in stoichiometric proportions and were dissolved in distilled water by a magnetic stirrer. Subsequently, when the metal salts were completely dissolved in the solution, citric acid was added to the precursor solution. The molar amount of citric acid was equal to a total molar amount of metal nitrates in the solution. This solution was heated to 80 °C on a heating plate with stirring for 2 hours using a magnetic stirrer, followed by the addition of ethylene glycol in a molar ratio of citric acid: ethylene glycol of 1: 4. Then, the solution was further heated to 110 °C to achieve the gel formation. For the auto-combustion step, the gel formation was put rapidly into electrical oven at temperature of 180 °C for 1 hour to obtain foamy dry powders, known as as-synthesized powders. These powders were grinded and calcined at the temperature of 900 °C for 2 hours in a muffle furnace to make the incompletely combusted part react thoroughly. The LSF powders were finally obtained.

2.3 Characterization

The phase and crystallinity of LSF powders were determined by powder X-ray diffraction (XRD) using a Philips X'Pert PANalytical X-ray diffractometer with Cu-K_α radiation (λ= 1.540598 Å) over Bragg's angles (2θ) ($10° \leq 2\theta \leq 80°$) at a step size of 0.02 and time/step of 1 s. The average crystallite size (D) of the samples was estimated using Scherrer's formula:

$$D = K\lambda/\beta cos\theta \quad (1)$$

where K is the shape factor of the average grain size (the expected shape factor is 0.89), λ is the characteristic wavelength (λ = 1.540598 Å) and β is the full width at half maximum of the X-ray peak. Field-emission scanning electron microscope (FESEM, JEOL JSM-6335F) with energy dispersive spectrum (EDS) facility was employed to study the microstructure characteristics of the LSF powders. The fourier transform infrared spectra (FTIR) were recorded using a Thermo Scientific Nicolet 6700 FTIR spectrometer. The photoluminescence (PL) property of the LSF powders was investigated by a fluoromax 4 spectrophotometer using excitation wavelength (λ_{ex}) of 310 nm at room temperature.

3. Results and discussion

Fig. 1 presents the XRD patterns of $La_{1-x}Sr_xFeO_3$ (x = 0.0, 0.2, 0.4, 0.6 and 0.8) samples calcined at 900 °C in the air atmosphere, compared with the JCPDS database No. 37–1493 and 40-0905 for $LaFeO_3$ and $SrFeO_{2.97}$ phases, respectively [15]. It was found that the main diffraction peaks of all samples are indexed according to the $LaFeO_3$ phase, indicating the single perovskite phase with an orthorhombic structure and no evidence of any impurity phases (Fig.1a). The Sr-doping up to 80% does not significantly affect the crystal structure of $LaFeO_3$. Fig. 1b shows the magnified XRD patterns of all the samples at the 2θ range between 30° and 35° including the reflection of the (121) plane. It is observed that the (121) peak is a significant shifting toward higher 2θ angle with increasing the amount of Sr dopant, which can be attributed to the lattice structure distortion induced by Sr doping [16, 17]. This is due to the substitution of the larger atomic radius of La (1.15 Å) by the smaller atomic radius of Sr (1.13 Å) [16, 18].

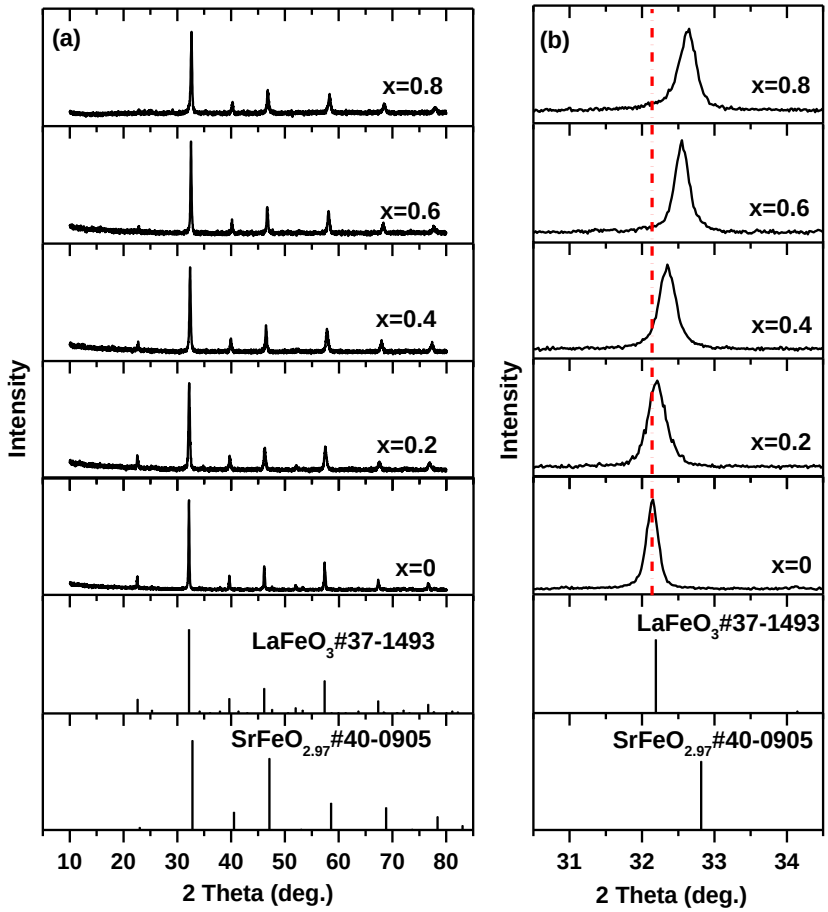

Figure 1. XRD patterns of the samples of $La_{1-x}Sr_xFeO_3$ (x = 0.0, 0.2, 0.4, 0.6 and 0.8).

The average crystallite size (D) of undoped and Sr-doped $LaFeO_3$ samples are summarized in Table 1. It can be seen that there is no significant difference in average crystallite size of the samples. The average crystallite size of undoped $LaFeO_3$ was found to be 37 nm, while the average crystallite size of Sr-doped $LaFeO_3$ was found to be 30.1, 32.5, 34.7 and 37.5 when x = 0.2, 0.4, 0.6 and 0.8 nm, respectively. The present average crystallite size of all the powders relatively close to those of the

undoped and doped $LaFeO_3$ prepared by sol-gel method [6, 17, 19]. So, undoped and Sr-doped $LaFeO_3$ perovskite powder have been successfully synthesized through sol-gel auto-combustion method.

Table 1. Crystallite size and particle size of the $La_{1-x}Sr_xFeO_3$ (x = 0.0, 0.2, 0.4, 0.6 and 0.8) samples.

Samples	Crystallite Size (nm)	Particle Size (nm)
$LaFeO_3$	37.9	264
$La_{0.8}Sr_{0.2}FeO_3$	30.1	153
$La_{0.6}Sr_{0.4}FeO_3$	32.5	222
$La_{0.4}Sr_{0.6}FeO_3$	34.7	212
$La_{0.2}Sr_{0.8}FeO_3$	37.5	238

To further ascertain the presence of LSF, FTIR technique was employed to obtain information about the chemical bonding in the material. The FTIR spectra of undoped and Sr-doped $LaFeO_3$ powders are shown in Fig. 2. The results exhibit relatively differences at the absorption peaks of 536 cm^{-1} which referred to Fe-O stretching vibration mode [6, 17]. The disappearance of the characteristic bands of Fe-O stretching mode of LSF with the increasing of Sr content revealed that the substitution of Sr in $LaFeO_3$ has a significant effect to Fe-O stretching vibration mode. However, Sr-O stretching mode at 864 and 859 cm^{-1} was not detected in all the LSF samples, compared to the $LaFeO_3$ and $La_{0.7}Sr_{0.3}FeO_3$ samples [17]. Moreover, there was no observation of absorption peaks at about 1300 and 1600 cm^{-1} which referred to carboxyl group and NO_3^- stretching mode, indicating that all the carboxyl group and the NO_3^- ion took part completely in the reaction during combustion.

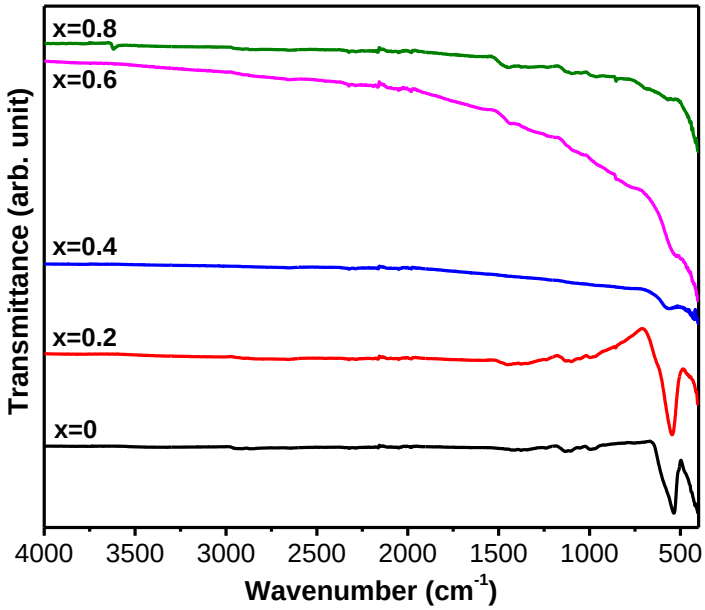

Figure 2. FTIR spectra of $La_{1-x}Sr_xFeO_3$ (x = 0.0, 0.2, 0.4, 0.6 and 0.8) samples.

The morphology of LSF perovskite particles evaluated by FESEM is shown in Fig. 3. It can be observed that all the synthesized LSF powders have an irregular shape with very uniform particle size distribution and small amount of agglomerations of particles. The average particle size of all the samples is summarized in Table 1. The average particle size of undoped $LaFeO_3$ was found to be 264 nm, while the average particle size of Sr-doped $LaFeO_3$ was found to be 153, 222, 212 and 238 when x = 0.2, 0.4,

0.6 and 0.8 nm, respectively. The present morphology of LSF powder is quite similar to that synthesized by citrate sol-gel route [17]. This indicates that there is no significant difference in surface morphology and particle size of LSF powders with the increasing Sr dopant, corresponding to the XRD results.

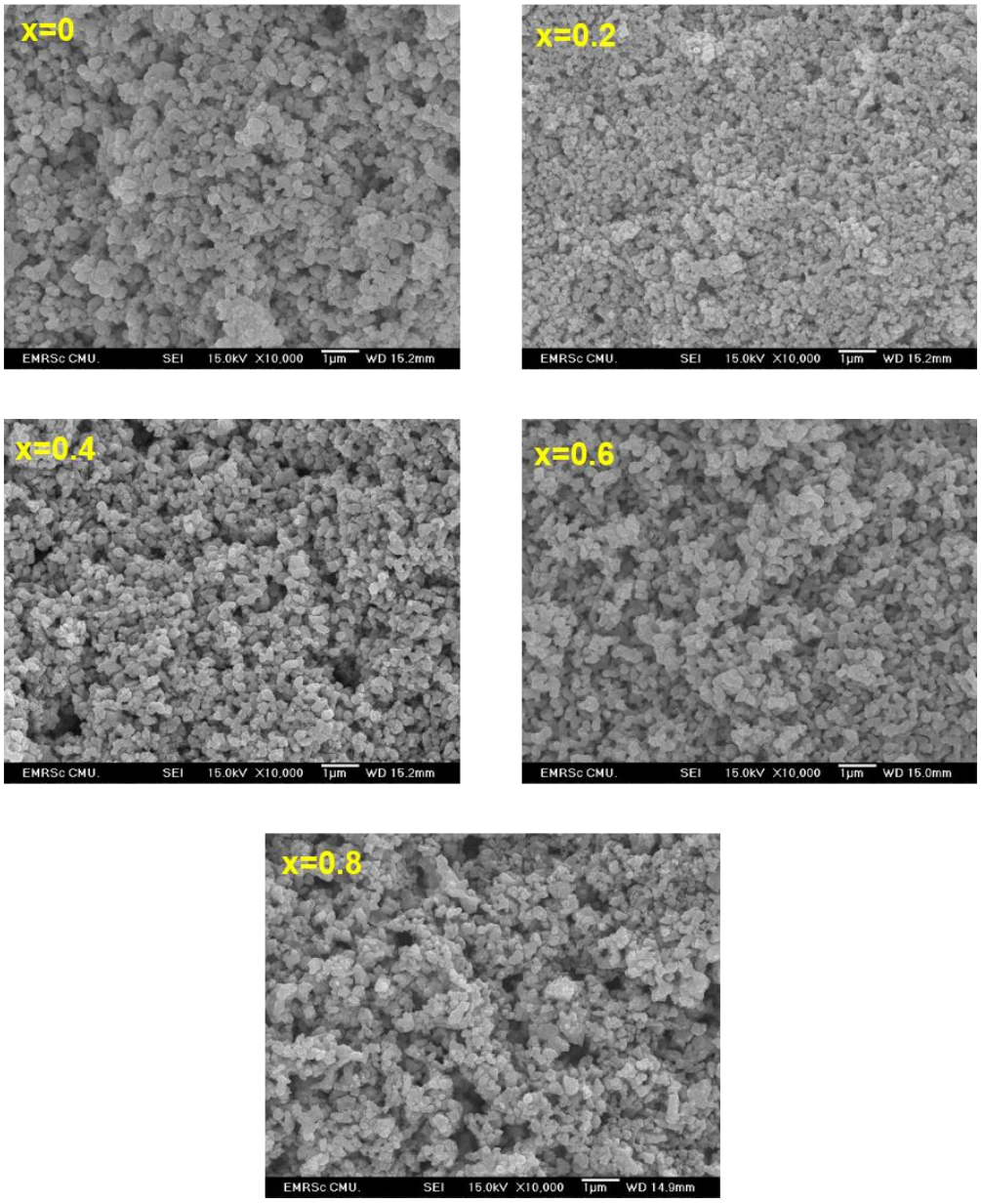

Figure 3. FESEM images of $La_{1-x}Sr_xFeO_3$ (x = 0.0, 0.2, 0.4, 0.6 and 0.8) samples.

To consider the chemical distribution and composition of LSF samples, FESEM-EDS with mapping analysis techniques were used to characterize the samples. Fig. 4 shows typical FESEM-EDS mapping of $La_{0.4}Sr_{0.6}FeO_3$ sample. The EDS mapping revealed that the sample consisted of detected La, Sr, Fe and O elements with relatively uniform distribution on the sample surface. The quantitative EDS analysis confirmed that the chemical composition was in good agreement with stoichiometric chemical

composition, as shown in Table 2. As for the other samples, similar results to those for $La_{0.4}Sr_{0.6}FeO_3$ sample were obtained.

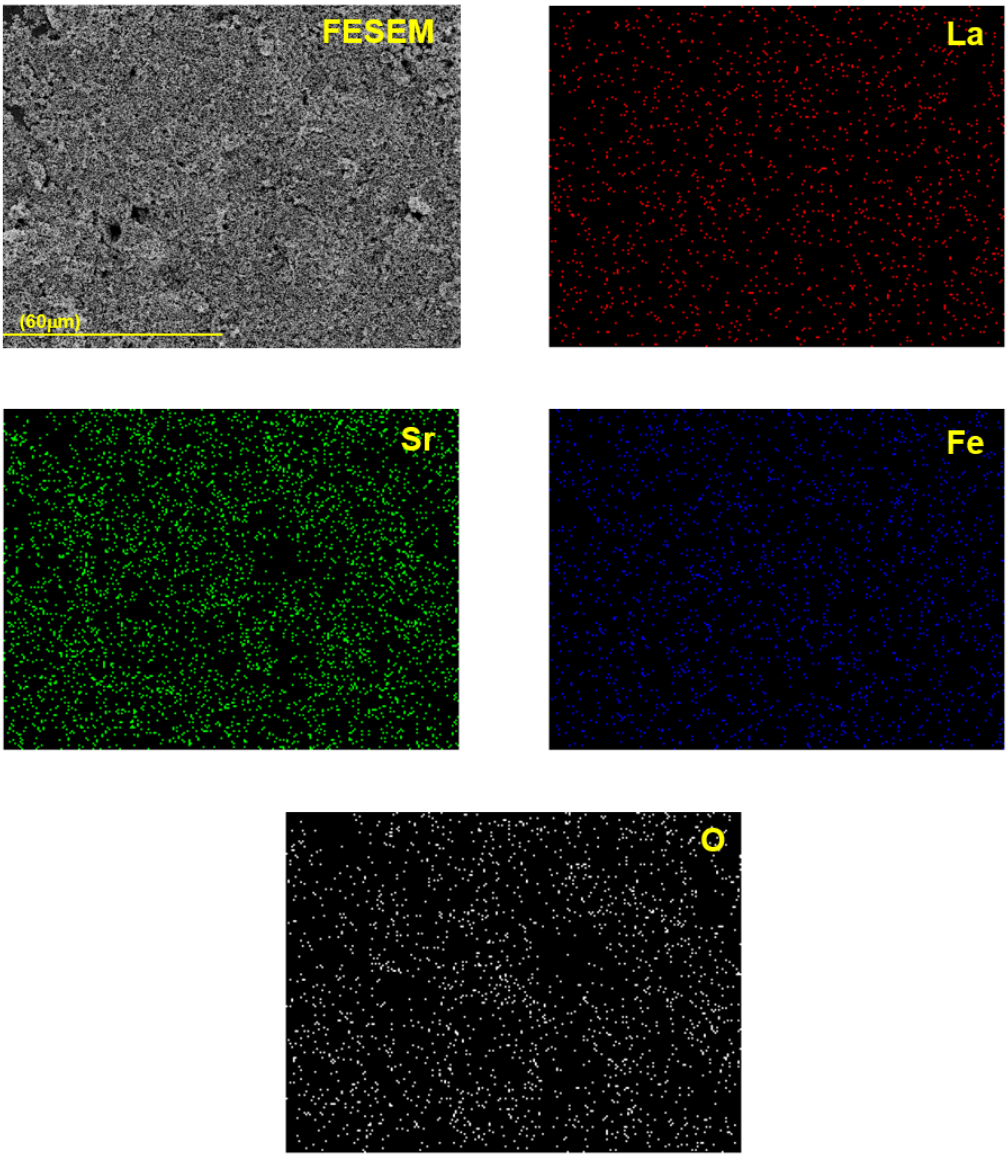

Figure 4. FESEM and EDS mapping images of $La_{0.4}Sr_{0.6}FeO_3$ sample.

Table 2. Elemental atomic composition of LSF samples through the EDS analysis.

Samples	Atomic (at.%)			
	La	Sr	Fe	O
$LaFeO_3$	24.68	0.00	22.45	52.80
$La_{0.8}Sr_{0.2}FeO_3$	17.10	4.55	20.23	58.13
$La_{0.6}Sr_{0.4}FeO_3$	15.41	9.35	21.82	53.42
$La_{0.4}Sr_{0.6}FeO_3$	9.15	14.28	20.13	56.44
$La_{0.2}Sr_{0.8}FeO_3$	4.58	18.26	20.41	56.74

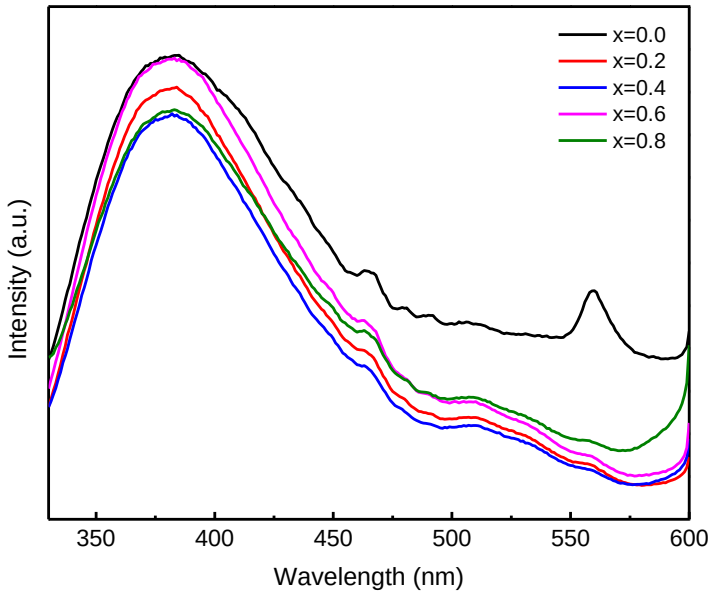

Figure 5. Photoluminescence spectra of $La_{1-x}Sr_xFeO_3$ (x=0.0, 0.2, 0.4, 0.6 and 0.8) samples.

To understand the diffusion and the recombination rate of photogenerated electron–hole pairs, PL spectroscopy was investigated. Generally, PL intensity is related to the recombination rate of electron–hole pairs. The low PL intensity implies the low recombination rate and the high separation rate of photogenerated carriers, resulting in the high photocatalytic activity under light irradiation. PL spectra of the as-synthesized $La_{1-x}Sr_xFeO_3$ (x=0.0, 0.2, 0.4, 0.6 and 0.8) particles excited at 310 nm wavelength are shown in Fig. 5. Undoped $LaFeO_3$ powder shows the emission peaks at around 380 and 560 nm. However, all the LSF powders show only the highest emission peaks at around 380 nm. The emission peak of the LSF samples disappeared at 560 nm probably due to a higher photocatalytic activity under light irradiation as results of Sr dopant [20].

4. Conclusions

In the present study, the undoped and Sr-doped $LaFeO_3$ (LSF) perovskite has been successfully synthesized by new route sol-gel auto-combustion method. XRD and FESEM results showed that the as-prepared LSF samples were single phase with no detection impurities and uniform size distribution. The Sr-doping up to 80% does not significantly affect the crystal structure and particle size of LSF. The FESEM-EDS mapping analysis showed that all samples consisted of detected La, Sr, Fe and O elements with relatively uniform distribution on the sample surfaces. In addition, the chemical composition of the

samples corresponded to stoichiometric chemical composition. The FTIR spectra revealed that the substitution of Sr in $LaFeO_3$ has a significant effect to Fe-O stretching vibration mode.

Acknowledgments
This work is supported by National Research Council of Thailand (NRCT) through Naresuan University (R2561B103), Phitsanulok, Thailand. Additional support was kindly provided by the School of Renewable Energy and Smart Grid Technology, Naresuan University, Thailand.

References
[1] Porta P, De Rossi S, Faticanti M, Minelli G, Pettiti I, Lisi L, and Turco M 1999 *J. Solid State Chem.* **146** 291
[2] Sunarso J, Hashim S S, Zhu N, and Zhou W 2017 *Prog. Energ. Combust.* **61** 57
[3] Rai A and Thakur A K 2017 *J. Alloy. Compd.* **695** 3579
[4] Lin Q, Xu J, Yang F, Yang X, and He Y 2018 *J. Appl. Biomater. Func.* **16** 17
[5] Díez García M I and Gómez R 2017 *ChemSusChem* **10** 2457
[6] Gosavi P V and Biniwale R B 2010 *Mater. Chem. Phys.* **119** 324
[7] Acharya S, Mondal J, Ghosh S, Roy S K, and Chakrabarti P K 2010 *Mater. Lett.* **64** 415
[8] Wang B, Yu Q, Zhang S, Wang T, Sun P, Chuai X, and Lu G 2018 *Sensor. Actuat. B-Chem.* **258** 1215
[9] Haron W, Wisitsoraat A, and Wongnawa S 2017 *Ceram. Int.* **43** 5032
[10] Zheng W, Liu R, Peng D, and Meng G 2000 *Mater. Lett.* **43** 19
[11] Dixon C A L, Kavanagh C M, Knight K S, Kockelmann W, Morrison F D, and Lightfoot P 2015 *J. Solid State Chem.* **230** 337
[12] Deganello F and Tyagi A K 2018 *Prog. Cryst. Growth Charact. Mater.* **64** 23
[13] González-Cortés S L and Imbert F E 2013 *Appl. Catal., A* **452** 117
[14] Yue Z, Zhou J, Li L, Zhang H, and Gui Z 2000 *J. Magn. Magn. Mater.* **208** 55
[15] Powder-diffraction-file, *JCPDS-ICDD*. 2001, 12 Campus Boulevard, Newton Square, PA 19073-3272, USA.
[16] Wang W, Lin B, Zhang H, Sun Y, Zhang X, and Yang H 2019 *J. Phys. Chem. Solids.* **124** 144
[17] Murade P A, Sangawar V S, Chaudhari G N, Kapse V D, and Bajpeyee A U 2011 *Curr. Appl. Phys.* **11** 451
[18] Kittel C, *Introduction to solid state physics*. 8th ed. ed. 2005, USA: John Wiley & Sonc.
[19] Del Toro R, Hernández P, Díaz Y, and Brito J L 2013 *Mater. Lett.* **107** 231
[20] Phuruangrat A, Wongwiwat N, Thongtem T, and Thongtem S 2018 *Res. Chem. Intermediat.* **44** 7427